



Cite this: *Nanoscale*, 2017, **9**, 9510

## Reinforcement of natural rubber latex using lignocellulosic nanofibers isolated from spinifex grass†

Alireza Hosseinmardi, <sup>a</sup> Pratheep K. Annamalai, <sup>a</sup> Lianzhou Wang, <sup>a,b</sup> Darren Martin <sup>\*a</sup> and Nasim Amiralian <sup>\*a</sup>

Reinforcement of natural rubber (NR) using nanofillers often results in an enhancement of the tensile strength, but at the expense of elongation at break and toughness. In this study, with the objective of strengthening NR without compromising its compliance, we investigate the reinforcement efficiency of a series of cellulose nanofibers (CNF) with variations in residual hemicellulose, lignin and therefore surface chemistry. Different types of high aspect ratio CNF isolated from *Triodia pungens* (*T. pungens*), an Australian arid grass commonly known as spinifex, were added at 0.1–2 wt% loadings into a pre-vulcanized NR latex. CNF/NR nanocomposites then were benchmarked against NR nanocomposites incorporating a well-known wood-derived CNF. It was found that the presence of residual lignin and hemicellulose, and the pretreatment with a deep eutectic solvent, a mixture of choline chloride and urea (CCU), could increase the compatibility of CNF with the NR matrix, while still enabling stability and handling of the colloidal latex mixture. Incorporation of 0.5 and 0.1 wt% of the sodium hydroxide treated CNF and choline chloride/urea treated CNF into the NR latex showed respectively 11 and 17% enhancement in tensile stress, and importantly without compromising viscoelastic properties; while addition of 0.1 wt% wood-derived CNF resulted in 18% decrease in both tensile stress and strain coupled with more pronounced latex stiffening.

Received 13th April 2017,  
Accepted 15th June 2017  
DOI: 10.1039/c7nr02632c  
rsc.li/nanoscale

## Introduction

Tough elastomers are a technologically critical class of materials used in many important industrial applications where they are required to deform reversibly to large strains.<sup>1–3</sup> Several approaches have been employed to enhance the toughness of elastomers, including the introduction of heterogeneities in the elastomeric host matrix, increasing viscoelasticity by macromolecular friction, partial or complete cross-linking of the elastomer, optimally tuning the average number of monomers in cross-linked chains and controlling energy dissipation to prevent crack propagation using both chemical synthetic and physical modification methods. However, it is fair to say that most of these approaches are limited by a cost, shelf life, process implementation, and scalability perspec-

tive.<sup>4,5</sup> Nanofillers represent an outstanding strategy to simultaneously enhance elastomer strength while retaining compliance, due to exponentially increasing the molecular friction and physical crosslinking, and also in some cases reducing the energy dissipation.<sup>6,7</sup> On the other hand, there is a growing demand from customers, government regulatory bodies and manufacturers that the new generation elastomers filled with nanofillers should be ideally based on sustainable raw materials using low-cost processing and without any occupational and health safety issues (for example, no organic or toxic solvent usage).<sup>8–10</sup>

Natural rubber (NR) is a bio-based polymer available in the form of latex, which has been utilized in the production of over 40 000 different products including tires, foams, sealants, gloves and condoms. Vulcanized (cured and cross-linked) NR has outstanding properties such as high elasticity, resilience, film forming capacity and hydrophobicity.<sup>11–13</sup> In order to develop the next generation of high-performance NR-based products, a variety of nanomaterials such as nanoclay, carbon nanotubes, graphene, and graphene oxide have been incorporated into latex, but their application is still somewhat limited by the sustainability, poor scalability and environmental and/or occupational health and safety concerns.<sup>14–17</sup> Therefore,

<sup>a</sup>Australian Institute for Bioengineering and Nanotechnology (AIBN), The University of Queensland, Brisbane 4072, QLD, Australia. E-mail: n.amiralian@uq.edu.au, darren.martin@uq.edu.au

<sup>b</sup>School of Chemical Engineering, The University of Queensland, Brisbane 4072, QLD, Australia

† Electronic supplementary information (ESI) available: Supplementary figures. See DOI: 10.1039/c7nr02632c

bio-based fillers such as starch, lignin, and cellulosic fillers have been explored in both micro and nano-scales dimensionality, due to their sustainability and excellent specific mechanical properties.<sup>18–21</sup> Current trends in the scientific literature highlight progressive improvements in the ultimate tensile stress of these NR nanocomposites reinforced with bio-based fillers. However, these strength increases are invariably associated with losses in compliance, elongation at break, and toughness.<sup>19,22–25</sup>

Recently, our team has isolated very high aspect ratio cellulose nanofibers (CNF) from spinifex grass, an abundant Australian arid grass, which covers about 27% of the continent. The special characteristics of this nanocellulose offer significant competitive advantages over CNF prepared from the other sources such as (1) a very high aspect ratio, (2) a uniquely high remnant hemicellulose content, even after bleaching (about 42 wt%), which engenders CNF hydrophobicity, flexibility, and toughness. This high hemicellulose content also greatly simplifies the conventional multi-step, often chemically aggressive production process, thus reducing energy demand and cost. In other words, the procedure to isolate CNF from spinifex has largely eliminated the typical chemical and mechanical pretreatment steps required in contemporary protocols.<sup>26–28</sup>

To achieve high-performance NR nanocomposite, dispersion quality and interfacial adhesion between nanofillers and host polymer are critically important.<sup>29</sup> In principle, the combination of a relatively hydrophobic NR matrix with typically hydrophilic cellulose fillers would be expected to suffer from a lack of interfacial compatibility. It has been demonstrated that presence of remnant lignin and hemicellulose can enhance the amphiphilic characteristics of CNF, resulting in superior dispersion, compatibility and reinforcement in polystyrene nanocomposites.<sup>30</sup>

In this study, we investigate the reinforcement performance of a series of unique spinifex CNF to enhance toughness and viscoelastic performance of industrial pre-vulcanized NR latex (it is very important to note here that commercially-acceptable, high quality grades will display a minimum tensile strength of over 20 MPa). Three different types of CNF with differing surface chemistries were prepared from *T. pungens* and their latex reinforcement performance benchmarked against a commercially available wood-derived CNF. In doing so, we successfully demonstrate that when the CNF-latex interface is engineered properly, a very desirable nanocomposite property profile showing increased strength and toughness, without detriment to stiffness, can be achieved.

## Experimental

### Materials

Pre-vulcanized NR latex with a total solids content of 60 wt% was supplied from Mardec Industrial Latex (Malaysia). Spinifex grass, *T. pungens*, was collected from Camooweal, north-west Queensland, Australia. Spinifex was washed with hot water

(80 °C) then dried at room temperature for 2–3 days. Sodium hydroxide (NaOH, Chem-supply), sodium chlorite (NaClO<sub>2</sub>, Sigma-Aldrich), ammonia (NH<sub>3</sub>, Chem-supply), urea (CH<sub>4</sub>N<sub>2</sub>O, Chem-supply), choline chloride (C<sub>5</sub>H<sub>14</sub>ClNO, Sigma-Aldrich), glacial acetic acid (CH<sub>3</sub>COOH, Ajax Finechem) and calcium carbonate (CaCO<sub>3</sub>, Omycarb™, Omya Australia pty.) were used as received. Wood-derived CNF was purchased from Process Development Centre of the University of Maine. This CNF was produced from softwood bleached pulp through the ultrafine grinder (mechanical refining, Masuko MKZB15-50J super mass collider) with no specific surface charge.<sup>31,32</sup>

### Preparation of cellulose nanofibers (CNF)

Three types of CNF with different surface properties were prepared from *T. pungens* (Fig. 1a). Ground and washed grass was soaked in DI water overnight and then delignified using a 2% (w/v) NaOH solution with a grass to solvent ratio of 1 : 10 at 80 °C for 2 h, followed by filtering and rinsing with 60 °C water.<sup>27</sup> This sample was named “NaOH-treated grass”. The first type of spinifex CNF “NaOH-CNF” was prepared by homogenizing a dilute dispersion (3–4 mg ml<sup>-1</sup>) of NaOH-treated grass for two passes at a pressure of 700 bar using a high-pressure homogenizer (HPH, GEA homogenizer, Panda 2 K NS1001L, GEA Niro Soavi S.P.A, Italy). The second type of spinifex CNF, “B-CNF”, was prepared by bleaching the NaOH-treated grass with a 1% (w/v) acidic solution of sodium chlorite at 70 °C (pH adjusted to 4 using glacial acetic acid) with a 1 : 30 w/v grass to solvent ratio for 1 h, followed by filtration and rinsing with 60 °C water. This bleaching process was repeated twice in order to completely remove the residual and dissolved lignin. Bleached fibers were further diluted with DI water to a 3–4 mg ml<sup>-1</sup> concentration and homogenized with two passes at a pressure of 700 bar.<sup>26,27</sup> A common deep eutectic solvent (DES) comprising a mixture of hydroxyl ethyl trimethyl ammonium (choline) chloride and urea at a molar ratio of 1 : 2 was employed to prepare the last type of spinifex CNF, which was called “CCU-CNF”. Briefly, the choline chloride and urea mixture was heated to 100 °C, then dried NaOH-treated grass was added to this clear DES to form a 1 wt% suspension, followed by gentle stirring for 2 h at 100 °C and sub-

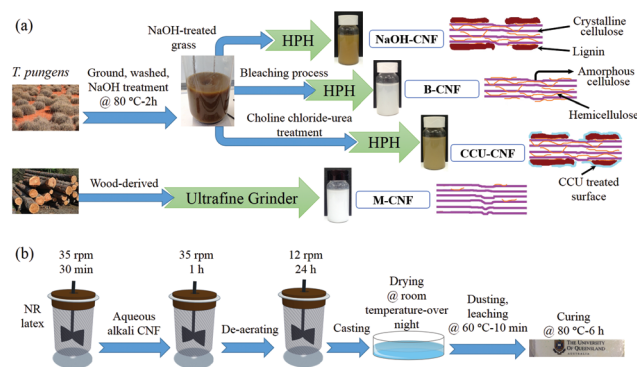


Fig. 1 The schematic of (a) CNF preparation from *T. pungens* and wood, (b) nanocomposite processing.

sequent dilution and rinsing with deionized water.<sup>33</sup> Similar to the other two spinifex CNF samples, DES-treated fibers were passed through the high-pressure homogenizer twice at a pressure of 700 bar. Wood-derived commercial CNF was purchased from the University of Maine and annotated as “M-CNF” to benchmark against the series of CNF prepared from *T. pungens*.

### Nanocomposite processing

The “control sample” NR host polymer and CNF/NR nanocomposites were conveniently prepared in a latex state as shown in Fig. 1b. To prepare the control sample, pre-vulcanized NR latex was stirred using an overhead stirrer for 30 minutes at a speed of 35 rpm. Then, it diluted to 45 wt% solids content using alkali aqueous ammonia solution at pH 10.5, followed by stirring for another 1 h at 35 rpm, and a further 24 h at 12 rpm to de-aerate the mixture. Complete series of CNF/NR nanocomposites with different CNF concentrations (0.1, 0.5, 1 and 2 wt%) were prepared by adding an aqueous dispersion of nanocellulose, again adjusted to pH 10.5 with ammonia and stirred for 30 minutes before adding to the latex so as to result in a mixture solids content of 45 wt%. The following mixing procedures were similar for all samples. It worth to mention that the viscosity of gel-like 2 wt% M-CNF and latex nanocomposite was clearly higher than the other nanocomposite dispersions. This observation will be seen in rheology properties of samples in the results and discussion section.

The control sample and stable latex CNF/NR mixtures were cast into a flat glass mold and dried overnight at room temperature. Dried films (thickness of 200 to 300 μm) were firstly dusted with calcium carbonate powder then leached for ten minutes in distilled water at 65 °C, followed by curing at 80 °C in a convection oven under a gentle purge of dry nitrogen for 6 h. Latex films were rested for at least 48 h at room temperature and 50% humidity before any further characterization.

### Characterization

**CNF characterization.** Transmission electron microscopy (TEM) at 80 kV (Hitachi HT7700) and high-resolution TEM at 200 kV (HR-TEM JEOL F20) were used to study the diameter and morphology of the spinifex CNF series and M-CNF. For the TEM observation, a small droplet of dilute CNF suspension was placed on a carbon-coated copper grid (which was glow discharged using a Cressington Carbon Coater (208 Carbon) at 15 mA for 15 s before use). After drying, the CNF samples were negatively stained with a drop of 2% (w/v) uranyl acetate (UA) for 10 min and images were captured on a SIS Morada 4 K CCD camera. Nanofiber diameters were reported as an average diameter measured from 50 different fibers using ImageJ software. For HR-TEM, hollow carbon coated Cu grids were used without glow discharge and staining.

Water contact angles of the nanopapers made of different CNF dispersions were measured to investigate the relative surface energy of the CNF. CNF films were formed on a commercial cellulose acetate membrane (45 μm pore size) by

vacuum filtration and dried between two Teflon sheets at 50 °C and ~20 kg weight overnight. The contact angle of the flat surface of nanopaper specimens was measured by sessile drop measurement (Dataphysics, OCA 15EC) and images were captured using a CCD camera (UEye®). Contact angle value were reported as an average of at least five droplets (5 μl) measured with Image J software on different positions. Infrared spectroscopy was carried out using a Nicolet 6700 spectrophotometer, equipped with an attenuated total reflectance (ATR) attachment in the wavenumber range of 400–4000 cm<sup>-1</sup> at 1 cm<sup>-1</sup> nominal resolution. Samples were dried in vacuum oven at 65 °C for 24 h to remove the majority of absorbed moisture before testing. Surface chemical bonding of all CNF was evaluated by X-ray Photoelectron Spectroscopy (XPS, ESCALAB220i-XL instrument (VG Scientific, UK)) using a monochromated Al Kα excitation source. The survey scan and high-resolution survey on C 1s and O 1s were performed.

**Control sample and nanocomposite characterization.** Rheological measurements of control and nanocomposite mixtures were performed in latex form at 25 °C with a shear rate of 0.1 s<sup>-1</sup> to 100 s<sup>-1</sup> using a TA Instruments (AR1500) rheometer fitted with 25 mm parallel plates.

To evaluate the mechanical properties of the nanocomposites, seven dumbbell-shaped specimens (18 × 2.5 mm) were cut and tested using an Instron 5543 fitted with a 500 N load cell at a crosshead speed of 500 mm min<sup>-1</sup>. Scanning electron microscopy (SEM, JEOL 7100) was used to observe the fracture surface of samples snapped with liquid nitrogen, as well as a cross section of the specimens after ambient uniaxial tensile testing. All of the specimens were coated with a thin layer (about 20 nm) of palladium prior to microscopic observation.

To investigate the swelling behavior of the CNF-NR nanocomposite series, the samples were first dried at 60 °C under vacuum for 24 h, then repeatedly weighed by digital balance (MX5, Mettler Toledo, *d* = 1 μm) until a constant weight was obtained. Then the samples were immersed in DI water at room temperature, and the water uptake was measured<sup>34</sup> at several time intervals (6 and 12 h, 1, 3, 7 and 14 days) of immersion. The specimens were removed from DI water and any adhering water droplets were blotted with filter paper without any excessive pressure on the surface of samples before re-weighing. The relative weight gain was measured and water uptake was calculated using the following equation:

$$\text{Water uptake(\%)} = \frac{W - W_0}{W_0} \times 100$$

where *W* and *W*<sub>0</sub> are the ultimate and initial weight of specimens, respectively.

## Results and discussion

### CNF variant

**Chemical properties.** Fig. 2 presents the ATR-FTIR spectra of the four different CNF. The peak in the range of 3000 to

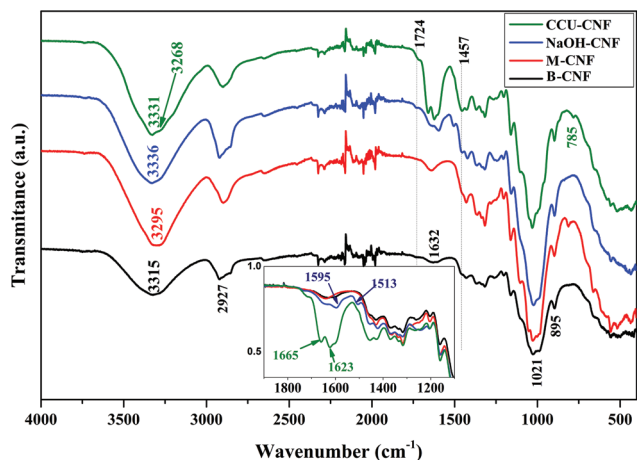


Fig. 2 FT-IR spectra of the different types of CNF (B-CNF, M-CNF, NaOH-CNF, and CCU-CNF).

3600  $\text{cm}^{-1}$  represents the hydroxyl stretching bond and the band at 1632  $\text{cm}^{-1}$  corresponds to the bending mode of the absorbed water. The peaks around 2920  $\text{cm}^{-1}$  (C–H stretching bond of alkane group), 1429  $\text{cm}^{-1}$  (symmetric bending of  $\text{CH}_2$ ), 1370  $\text{cm}^{-1}$  (C–H or O–H bending), 1317  $\text{cm}^{-1}$  ( $\text{CH}_2$  wagging), 1280  $\text{cm}^{-1}$  (CH deformation in cellulose I), 1208  $\text{cm}^{-1}$  (C–O–C symmetric stretching, OH plane deformation), 1021  $\text{cm}^{-1}$  (stretching of C–O) and 895  $\text{cm}^{-1}$  (C–O–C stretching at the  $\beta(1 \rightarrow 4)$ -glycosidic linkage) observed in all CNF.<sup>26,35–37</sup>

Peaks at 1457  $\text{cm}^{-1}$  ( $\text{CH}_2$  bending) and 1725  $\text{cm}^{-1}$  (C=O stretching vibration) show a higher intensity for NaOH-CNF and CCU-CNF in comparison with B-CNF and M-CNF. These two peaks are representative of aromatic groups associated with the lignin components. For NaOH-CNF, the peak around of 2927  $\text{cm}^{-1}$  (asymmetric methoxyl C–H stretching bonding) shows the highest intensity among all other samples, indicating the higher lignin content.<sup>38–40</sup> The hydroxyl stretching bond at 3336  $\text{cm}^{-1}$  and 3331  $\text{cm}^{-1}$ , is observed for the NaOH-CNF and CCU-CNF variants, respectively. After bleaching (B-CNF) this peak shifts to 3315  $\text{cm}^{-1}$  and for the M-CNF the OH stretching peak appears at 3295  $\text{cm}^{-1}$ . Shifting in the position of –OH stretching bond to a lower wavelength, indicates a higher degree of hydrogen bonding between the cellulose chains in bleached nanofibers in comparison to the NaOH-CNF.<sup>41</sup> The peak at 813  $\text{cm}^{-1}$  only appears in M-CNF which is associated with the glucomannan,  $\beta$ -D-glucose as a monomer available in the wood-derived cellulose structure.<sup>42,43</sup> Furthermore, FT-IR peaks at 665  $\text{cm}^{-1}$  (C–OH out-of-plane bending), 1001  $\text{cm}^{-1}$  (C–C, C–OH, C–H ring and side group vibration), 1053  $\text{cm}^{-1}$  (C–O–C asymmetrical stretching bond) and 1107  $\text{cm}^{-1}$  (C–O asymmetric valence vibration) are obviously more pronounced in M-CNF.<sup>40,43,44</sup> This indicates that M-CNF comprises cellulose chains with stronger hydrogen bonding, which arises from the formation of higher purity cellulose fibers.

The peaks at 1595 and 1513  $\text{cm}^{-1}$  in NaOH-CNF are associated with the aromatic in-plane ring bond stretching (aromatic

Table 1 Elemental analysis of the different types of cellulose nanofibers from the XPS typical survey spectra

| CNF types | O (at%)    | C (at%)    | N (at%)   | Si (at%)  | Ca (at%)  | O/C       |
|-----------|------------|------------|-----------|-----------|-----------|-----------|
| NaOH-CNF  | 25.3 ± 0.8 | 72.3 ± 3.2 | 0.3 ± 0.4 | 1.6 ± 2.1 | 0.4 ± 0.3 | 0.3 ± 0.0 |
| B-CNF     | 33.3 ± 1.7 | 65.1 ± 1.4 | 0.3 ± 0.5 | 1.3 ± 1.2 | 0         | 0.5 ± 0.1 |
| CCU-CNF   | 27.8 ± 3.5 | 70.9 ± 3.2 | 1.0 ± 0.5 | 0.3 ± 0.3 | 0         | 0.4 ± 0.1 |
| M-CNF     | 35.6 ± 1.4 | 63.0 ± 1.2 | 0.6 ± 0.1 | 0.7 ± 0.2 | 0         | 0.6 ± 0.0 |

C=C stretching) vibration of lignin.<sup>45</sup> In CCU-CNF, the absorption peaks at 1623  $\text{cm}^{-1}$  and 3268  $\text{cm}^{-1}$  showing N–H stretching and bending bonds of amide groups, respectively. The peaks at 785  $\text{cm}^{-1}$  and 1665  $\text{cm}^{-1}$  present C=O wagging and stretching, respectively, from the amide group.<sup>46,47</sup>

**Surface chemical properties.** XPS spectroscopy was employed to quantify the elemental surface composition of the CNF series. The relative mean elemental atomic percentage for the surface (five different spots) of different CNF types is presented in Table 1. Carbon and oxygen dominate the atomic percentage in all samples; however, the ratios of certain elements can shed light on the effect of CNF processing on surface chemistry.

The presence of silicon is generally well-known in crops as it is taken up by the roots of plants in the form of silicic acid and can be deposited in cell wall structures as an amorphous silica, hydrated silica and silicate (complex with mineral metals (such as Ca and Mg)).<sup>48–50</sup> It can be seen that the atomic percentage of silicon is 1.6% in NaOH-CNF and after bleaching, this value is reduced to 1.3%. The amount of silicon in CCU-CNF after treating with the choline chloride–urea mixture was also reduced to 0.3%. On the surface of NaOH-CNF a minor amount of calcium was also detected, which supports the retention of silicate complexes in this sample. The higher amount of nitrogen in CCU-CNF is clearly related to the second stage treatment of NaOH treated *T. pungens* by choline chloride–urea. It is known that the theoretical O/C ratio for pure cellulose, hemicellulose and lignin are 0.83, 0.81 and 0.33, respectively,<sup>51</sup> so increasing the value of O/C can be directly related to the extent of lignin removed from the surface of CNF. It can be seen that B-CNF and M-CNF were showing a higher O/C ratio compared to the alkali and DES-treated CNF (See Fig S1†).

Fig. 3 illustrates the high-resolution C 1s (Fig. 3a to d) and O 1s (Fig. 3e to h) spectra for NaOH-CNF, B-CNF, CCU-CNF, and M-CNF, respectively. Generally, the C 1s spectra can be fitted by four main peaks, C1 to C4. C1 appears at around 285 eV binding energy and corresponds to aromatic and aliphatic carbon backbone (carbon atoms with no oxygen neighbors), which in these samples represent the non-cellulosic components that are known to exist in adventitious carbon, lignin and extractives (fatty acids and resins).<sup>52–54</sup> The binding energy of C–O, C=O/O–C–O, and O–C=O/C≡O are associated with C2, C3, and C4 peaks, respectively.<sup>53,55</sup> All of the charge shifts for XPS data were corrected by using the binding energy of C–O (C2) bond based on the pure cellulose at 286.73 eV as a reference peak.<sup>56,57</sup> In this plot and Fig. S1,† the observed

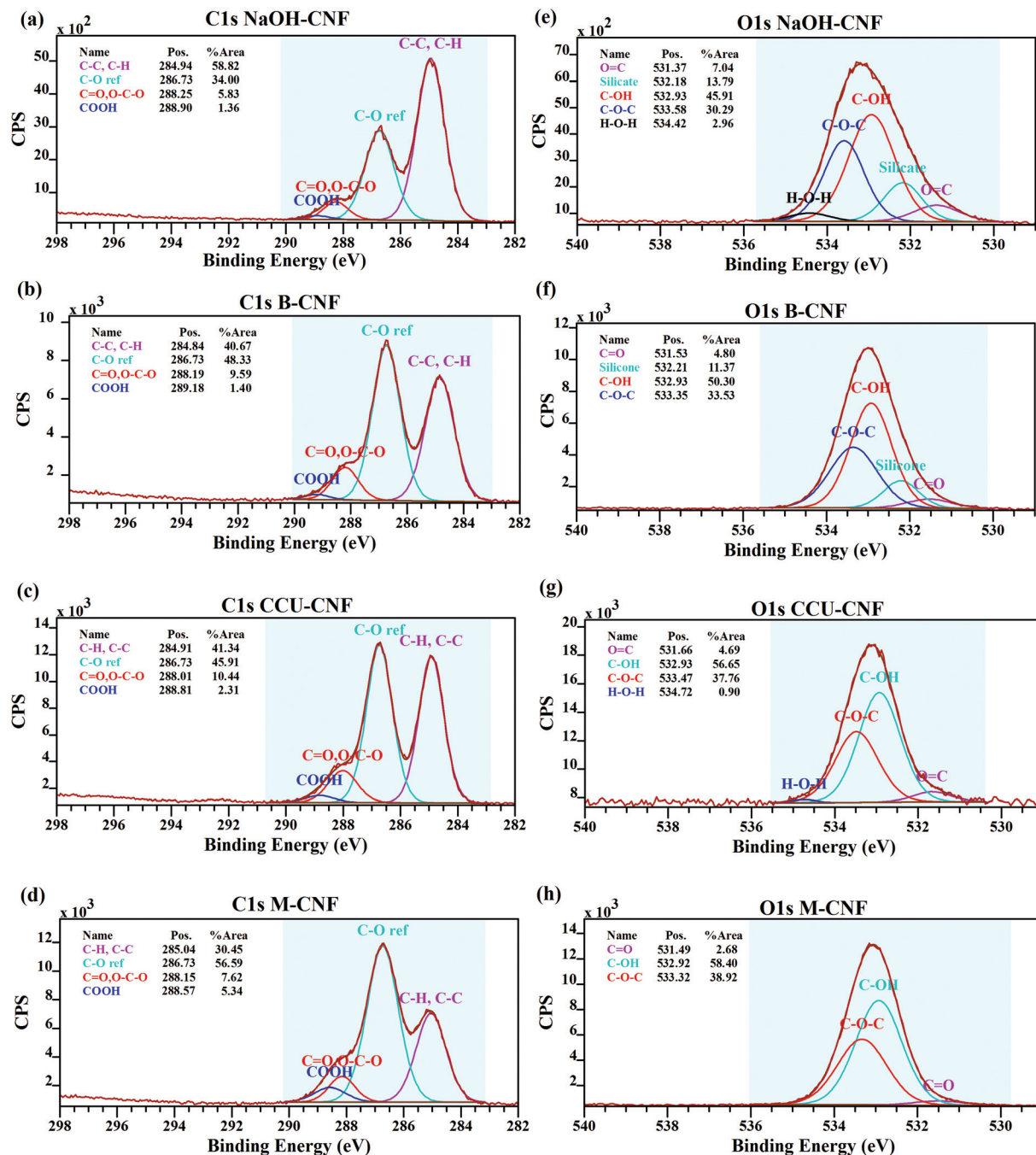







Fig. 3 High-resolution XPS carbon and oxygen spectra for different CNF types (a). C 1s for the NaOH-CNF, (b) C 1s for the B-CNF, (c) C 1s for the CCU-CNF and (d) C 1s for the M-CNF, (e). O 1s for the NaOH-CNF, (f) O 1s for the B-CNF, (g) O 1s for the CCU-CNF and (h) O 1s for the M-CNF.

decrease in the C1 bonding in high-resolution C 1s spectra with increasing O/C ratio directly relates to the degree of removal of extractives and/or lignin from the surface of the CNF series. Accordingly, the surface chemistry of NaOH-CNF shows more similarity to lignin. The bleaching process increases the O/C ratio while decreasing the C–C bonding, so the bleached CNF surface bears more similarity to a pure cellulosic surface. The lower intensity of C–C bonding in M-CNF compared to B-CNF indicates the inclusion of less lignin and

hemicellulose on the surface of M-CNF, as might be expected for a pure wood-derived CNF prepared using more intense common pulping methods.

The fitted high-resolution O 1s XPS spectra are presented in Fig. 3e to h. These spectra are calibrated based on the bonding of C–OH at 532.93 eV and its ratio to C–O–C bonding has been fixed at 60:40.<sup>57</sup> Silicate and silicone can be detected in NaOH-CNF and B-CNF at around 532 eV (ref. 58) binding energy, but these signatures are not seen in CCU-CNF and

**Table 2** Contact angle values and photographs of water droplets on the surface of NaOH-CNF, B-CNF, CCU-CNF and M-CNF

| Sample name                 | NaOH-CNF  | B-CNF   | CCU-CNF  | M-CNF   | Control sample NR   |
|-----------------------------|---|---|--|---|---|
| Contact angle ( $\theta$ )  | $45^\circ \pm 4.6^\circ$  | $30^\circ \pm 3.5^\circ$  | $62.7^\circ \pm 5.1^\circ$   | $8.6^\circ \pm 1.4^\circ$   | $82.7^\circ \pm 3.1^\circ$  |
| Photograph of water droplet |  |  |  |  |  |

M-CNF, which were given in the XPS survey spectra. The minor peaks present at around 531.3–531.6 eV are related to C=O bonding and can be related to the presence of lignin, hemicellulose and/or amide groups (especially in CCU-CNF, which was also present in the FT-IR spectra and relates to the absorption or adsorption of urea). The existence of amide groups in CCU-CNF is also confirmed by high-resolution N 1s (see Fig. S2†) showing a single peak at 400 eV.<sup>55</sup>

**Surface physical properties.** The contact angle measurement can provide further insights regarding the surface tension and wettability of CNF and NR control sample (Table 2).

M-CNF gave rise to the lowest contact angle ( $\theta = 8.6^\circ$ ) indicating the most polar surface among all of the samples. The contact angle of B-CNF is significantly higher at  $30.4^\circ$ . This is undoubtedly related to the presence of a higher content of hemicellulose and a small amount of residual lignin (3 wt%) in this CNF variant.<sup>26</sup> As discussed in FT-IR and XPS studies, the lignin content of NaOH-CNF is higher than the other CNF. Lignin comprises both hydrophobic and hydrophilic functional groups, which overall contribute to a higher contact angle compared to the pure cellulosic materials.

The DES system as a cationic functionalization pretreatment on NaOH-treated grass further increased the hydrophobicity of the CCU-CNF nanopaper, where  $\theta$  was measured at  $62.7^\circ$ . This could be related to the presence of amide groups on the surface, but may also be related to the softening and plasticizing effect of the DES on the components of NaOH-treated grass. We postulate that this plasticizing effect could accommodate the formation of a denser and smoother nanopaper surface, which in turn can affect contact angle. For completeness, the contact angle of the cured host NR polymer was measured at  $82.7^\circ$ , which is in agreement with literature values.<sup>59,60</sup> Thus, it can be seen that the contact angle value of CCU-CNF is closer to NR with respect to M-CNF and B-CNF.

**Dimensions.** Fig. 4a–d show the low and high-resolution TEM images of the CNF series. The average diameter of NaOH-CNF, B-CNF, CCU-CNF and M-CNF are  $12.6 \pm 2.5$  nm,  $12.5 \pm 3.8$  nm,  $10.7 \pm 2.7$  nm and  $15.8 \pm 6.7$  nm, respectively. In comparison, the choline chloride–urea treated spinifex nanofiber exhibits the smallest diameter, presumably due to positive charge repulsion, whereas the wood based M-CNF sample is comprised of relatively thicker nanofibers. The thicker dimensions of M-CNF could be attributed to the difference in the source, native structure, and fibrillation method. In the case of M-CNF, pure cellulose has a higher density of hydroxyl groups which may facilitate CNF agglomeration.<sup>61</sup>

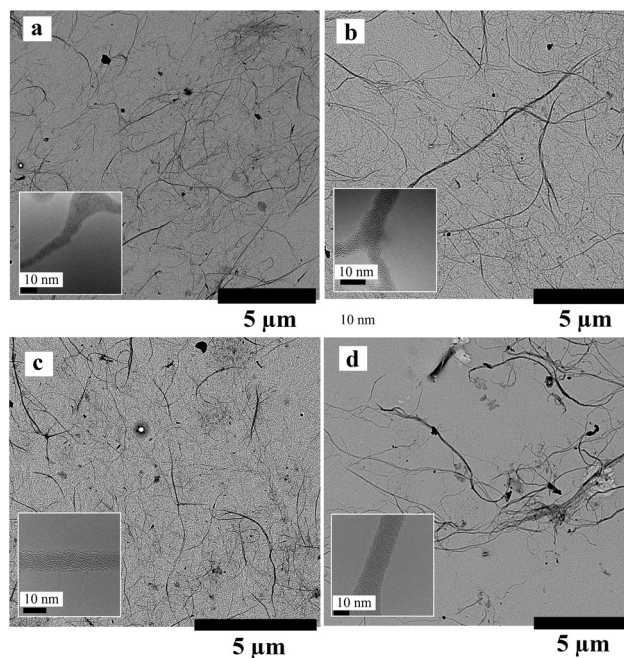


**Fig. 4** Transmission electron micrographs (scale bar 5  $\mu\text{m}$ ) of (a) NaOH-CNF, (b) B-CNF, (c) CCU-CNF and (d) M-CNF. Insets show the high-resolution TEM (HR-TEM) images (scale bar 10 nm).

### Rheology of NR/CNF suspensions

In order to understand the degree of compatibilization and dispersion of CNF in the latex colloidal suspension and the flow-behavior, the rheological properties of CNF/NR latex mixtures (at 0.1–2 wt% loading) were measured. In general, at room temperature, with increasing concentration of CNF, the zero-shear viscosity (or an initial shear viscosity at  $0.1 \text{ s}^{-1}$ ) of suspensions was increased (Table S1†) and a non-linear, shear-thinning non-Newtonian behavior was observed with increasing shear rate (Fig. 5).

The shear viscosity for the NR latex control sample at the initial shear rate at  $0.1 \text{ s}^{-1}$  was  $0.21 \text{ Pa s}$  and this was seen to decrease steadily with increasing shear rate, presumably due to the increased ease-of-flow of latex particles past one another with increasing the shear rate. Generally this shear thinning behavior is retained for suspensions with a 0.1 wt% loading of NaOH-CNF, B-CNF, and CCU-CNF indicating that the CNF are dispersed well among the NR latex particles without any significant interactions. However at higher loadings there are some changes in the rheological behavior, including an

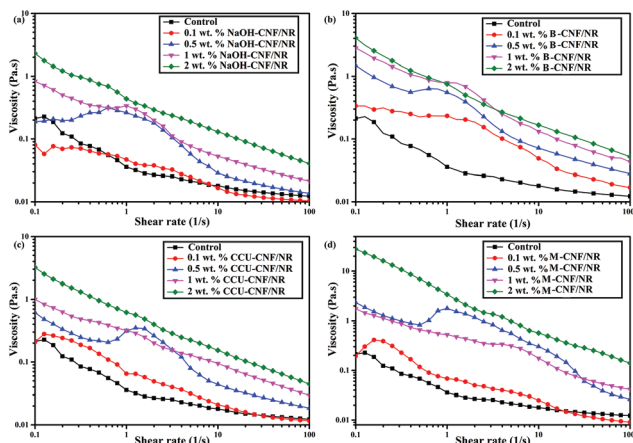


**Fig. 5** Viscosity versus shear rate of various weight concentration of different CNF (a. NaOH-CNF, b. B-CNF, c. CCU-CNF, and d. M-CNF) in NR latex.

increase in suspension viscosity due to the increased interaction of latex particles and cellulose nanofibers which restricts the mobility or ‘flow-ability’ of the latex particles.<sup>39,62</sup> Some of the CNF/NR latex suspensions, such as NaOH-CNF/NR at 0.5 and 1 wt% loadings, B-CNF/NR at 0.1, 0.5 and 1 wt% loadings, CCU-CNF/NR at 0.5 wt% and M-CNF at 0.1 and 0.5 wt% loadings in particular, display yield stress behavior, seen as a hump in the viscosity-shear rate curves and ascribed to more substantive inter-particle interactions, which need to be overcome in order for the suspension to flow. This yield behavior could, for example, be attributed to the formation of a layer of CNF around the NR latex particles. In a certain concentration range of CNF (which is specific for each type of fibers and could be related to its surface hydrophilicity, functional group and dimension), the latex particles interact well with nanofibers through cohesive forces to form a network in the suspensions, however at higher CNF concentrations, rather than forming this network larger discrete, agglomerates form preferentially and the yield stress behavior is concomitantly lost. For all CNF in the series, the yield stress signature disappeared at 2 wt% CNF concentration due to this phenomenon. The initial viscosity at  $0.1 \text{ s}^{-1}$  for the 2 wt% M-CNF/NR is significantly higher than that measured for other samples (27.7 Pa s), perhaps an indirect indicator of a higher degree of CNF agglomeration, higher latex composite stiffness and poor ultimate tensile properties in the cured films.

### Tensile properties of NR/CNF nanocomposites

Reinforcing pre-vulcanized latex systems with fillers is exceedingly challenging because successful reinforcement, in other words, the effective transfer of shear stress from matrix to filler, can only happen at the boundary between pre-cross-linked microscale latex particles after film formation and final curing, and all of this must not change the colloidal stability of suspension so that products can be manufactured (for example dipped condoms or gloves). In addition, if filler load-

ings are too high, latex-latex interparticle coalescence and adhesion can be masked, leading to a pronounced loss in ductility. The reinforcement efficiency of CNF at different concentrations was studied by measuring the uniaxial tensile properties of the series of nanocomposites. Fig. 6 summarizes the ultimate tensile strength, strain at break, toughness (calculated from the area under the stress-strain curves) and stress at 500% strain (an industry norm for comparing the stiffness of elastomers) values (also, see Fig. S3, Fig. S4, Fig. S5 and Table S2 in ESI† for the statistical distribution of these values).

The tensile strength, elongation at break and toughness values for the NR control sample are 24.3 MPa, 1925% and  $125 \text{ MJ m}^{-3}$ , respectively, showing very good mechanical properties of the host polymer compared to the majority of academic reports.<sup>20,63–65</sup> Nanocomposites reinforced with 0.1 and 0.5 wt% NaOH-CNF and 0.1 wt% CCU-CNF showed a 5.5%, 11.3% and 17% improvement in tensile strength, respectively, and importantly this was achieved without a significant decrease in tensile strain at break due to superior dispersion and interfacial compatibility between these more hydrophobic CNF variants and the NR host. The composite reinforced with 0.1 wt% CCU-CNF actually showed the highest reinforcement efficiency coupled with negligible stiffening and loss of elongation at break, but at higher loadings of this CNF variant, we suspect that DES treatment led to the plasticization of the CNF components,<sup>66</sup> perhaps resulting in the formation of softer CNF agglomerates with less mechanical integrity. The negligible stiffening displayed supports this supposition. The next most hydrophilic CNF in the series, bleached spinifex nanofibers, B-CNF, resulted in poor overall mechanical performance, with the most crystalline and hydrophilic wood-derived M-CNF showing the highest stiffening coupled with the most detrimental drops in strength, ductility and toughness. Bleached fibers have more tendency to agglomerate upon latex film drying due to their strong hydrogen-bonding propensity, which we believe most likely results in a heterogeneous distribution of nanofibers in the latex matrix, and ultimately the for-

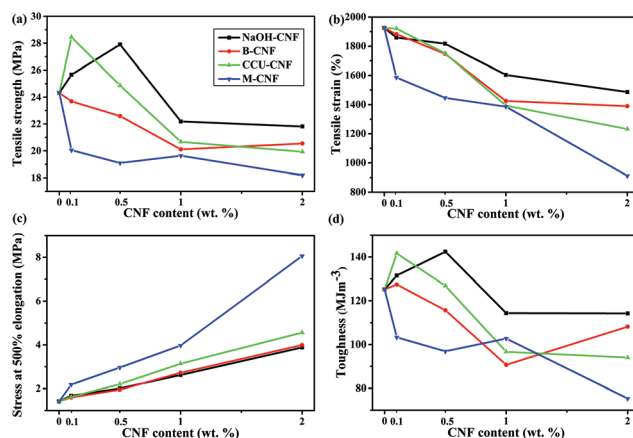


**Fig. 6** (a) Tensile strength, (b) elongation at break, (c) stress at 500% elongation and (d) toughness of NR nanocomposites with various CNF types and concentrations.

mation of larger stiff, but poorly compatibilized agglomerates, which can act as stress raisers. The increase of tensile stress above 3 MPa in the range of 100–500% elongation is one of the major drawbacks for NR latex nanocomposites. Retaining membrane compliance is a critical factor for high performance elastomer applications such as condoms and gloves. Overall, the latex membranes reinforced with less than 0.5 wt% *T. pungens*-based CNF retained this desirable softness, whereas the wood-derived CNF (M-CNF) were associated with a significant and undesirable stiffening effect. This stiffening effect is further exemplified in the DMA analysis (see Fig. S6†). Clearly, the mechanical data shows that CNF comprising carefully controlled remnant hemicellulose and lignin cell wall polymers can be advantageously employed to preserve ductility and compliance, while efficiently achieving considerable gains in strength and toughness. It is also particularly attractive that these results have been achieved without the use of additional organic dispersing agents, crosslinking agents or surfactants.

### Fracture surfaces and water uptake studies

Fig. 7a–e compare the SEM cross-sectional images of the cryo-fractured 0.1 wt% CNF/latex nanocomposites and Fig. 7f–j show SEM images of the fracture surface of the same nanocomposites after uniaxial tensile testing. With respect to the NR control sample which shows well-defined microscale latex globules or pits, the addition of nanocellulose variants is accompanied by some very interesting changes in fracture surface texture. The two best performing nanocomposites at this low loading (0.1 wt% NaOH-CNF and CCU-CNF) displayed a combination of both smoother cryo-fracture surfaces and tensile fracture surfaces more devoid of microscale pitting. This, plus the inclusion “wavy groove” features indicating well-compatibilized microscale CNF bundles all point towards better reinforcement and cohesion. The more hydrophilic variants (0.1 wt% B-CNF and M-CNF) showed a lot of pitting and de-bonding in the tensile fracture surfaces, together with evidence of larger, poorly-integrated agglomerates in the M-CNF composite, as might be expected.

The degree of water uptake of nanocomposites in DI water as a function of CNF type and loading is shown in Fig. 8. Although all samples including the control sample absorbed water, it can be seen that adding CNF into the NR matrix can significantly affect the kinetics of water uptake. Indirectly, this can tell us about the quality of dispersion and degree of connectivity of CNF bundles in each composite system. For example, some nanocomposites with 0.1–0.5 wt% loadings reached the plateau (corresponding to the water uptake at equilibrium) within 1–4 days compared to 7 days for the control sample due to the hydrophilic nature of cellulose which can form channels through the latex polymer matrix.<sup>67</sup> In general, the addition of 0.1 wt% CNF into the NR matrix resulted in the maximum level of water uptake after 14 days, regardless of the CNF type. For example 0.1 wt% NaOH-CNF/NR and 0.1 CCU-CNF/NR absorbed 44 and 31%, respectively more water than the control sample. Conversely, further increases in the concentration of CNF decreased the ultimate

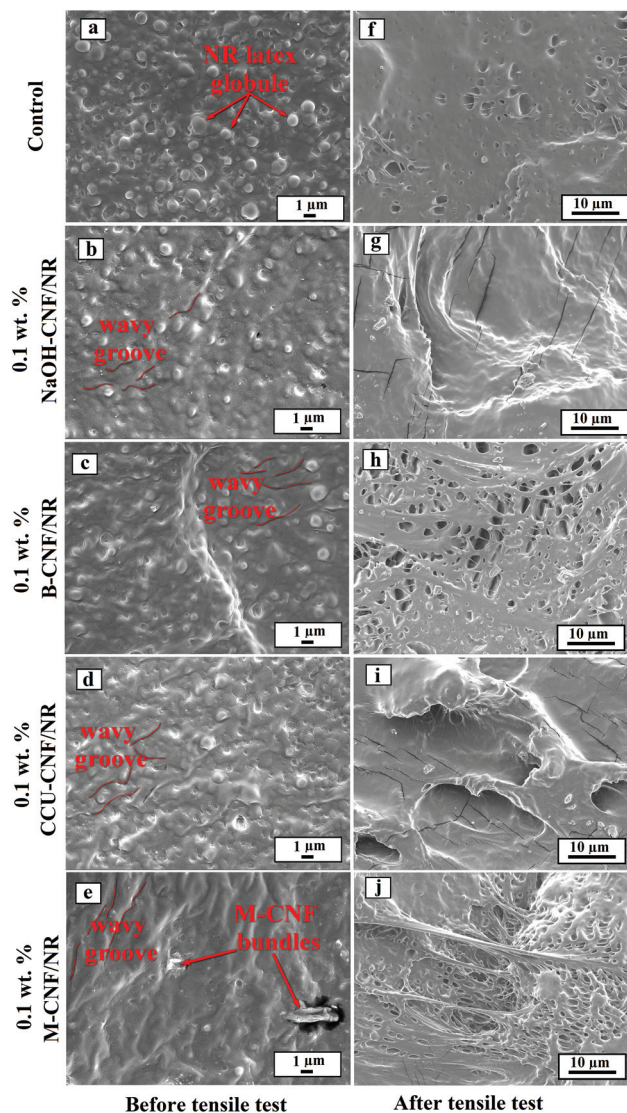
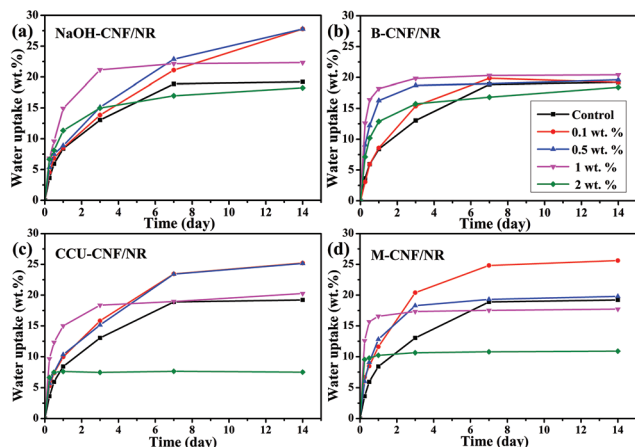


Fig. 7 SEM fracture surface of control sample and nanocomposites with 0.1 wt% of CNF/NR variants before (left) and after (right) tensile test.

swelling degree, and this was attributed to the formation of a coarser cellulose network (percolation network) that then behaves more as a barrier phase rather than a conduit, and therefore limits water diffusion.<sup>68</sup>

Behavior at the lower nanofiller loadings is particularly informative. The plateau for 0.1 and 0.5 wt% of B-CNF/NR and M-CNF/NR nanocomposites was achieved in less than a week, in contrast to 0.1 and 0.5 wt% of NaOH-CNF/NR and CCU-CNF/NR nanocomposites, which were still absorbing water after 2 weeks. This phenomenon could be related to the presence of more residual hydrophobic lignin in NaOH-CNF and CCU-CNF, which absorbs water slower than cellulose. In addition, it can be concluded that at low loadings of CNF (0.1 and 0.5 wt%) the strength of fiber–fiber interactions and degree of agglomeration in NaOH-CNF and CCU-CNF were lower than B-CNF and M-CNF nanocomposites. Therefore, it





**Fig. 8** Evolution of water uptake for NR nanocomposites with different CNF types and concentration (a. NaOH-CNF/NR, b. B-CNF/NR, c. CCU-CNF/NR and d. M-CNF/NR) as a function of time (0.5, 1, 2, 3, 7 and 14 days.) at room temperature.

can be assumed that the NaOH-CNF and CCU-CNF were dispersed better in these nanocomposites, which is in agreement with our rheology and tensile results, as well as SEM images. NR nanocomposites with 2 wt% CNF show the lowest water uptake capacity, which could be related to more extensive CNF agglomeration (see Fig. S7<sup>†</sup>).

## Conclusions

Here we reported the performance and characterization of a series of nanocomposites of natural rubber latex incorporating four different CNF variants, including three spinifex-derived CNF. We demonstrated the influence of CNF surface chemistry, dimensions and remnant lignocellulosic components. The incorporation of 0.5 wt% NaOH-CNF into a high-quality industrial pre-vulcanized NR latex grade has enhanced the tensile strength by 11% and the excellent dispersion and compatibility of this CNF grade are facilitated by the presence of residual lignin. The incorporation of CCU-CNF that originated from a deep-eutectic solvent (choline chloride and urea) pre-treatment protocol, and which exhibited a relatively higher surface hydrophobicity, resulted in the toughest nanocomposite. Due to its enhanced interfacial wettability/adhesion, the nanocomposite incorporating 0.1 wt% CCU-CNF enhanced the tensile strength by 17%, coupled with negligible stiffening and loss of elongation at break. Bleaching treatment (or removal of remnant lignin) of the spinifex pulp and resultant CNF resulted in inferior nanocomposite tensile properties. However, in comparison with a wood-derived bleached CNF (M-CNF), the nanocomposites with bleached spinifex CNF (B-CNF) demonstrated less stiffening and a less severe reduction in tensile properties, which is attributed to the higher hemicellulose content in B-CNF. It can be concluded that through careful, systematic control of the residual hemicellulose and lignin components in the CNF structure, NR

latex nanocomposites with attractive property profiles can be prepared with enhanced CNF dispersion and interfacial adhesion, as well as no expected occupational and health safety issues.

## Acknowledgements

The authors appreciatively acknowledge the Australian government for international postgraduate research scholarship (IPRS) and University of Queensland continental scholarship. The authors would like to admit the facilities of the Australian Microscopy and Microanalysis Research Facility at the Centre for Microscopy and Microanalysis, the University of Queensland and Dr. Barry Wood for taking XPS spectra.

## References

- 1 M. K. Shin, G. M. Spinks, S. R. Shin, S. I. Kim and S. J. Kim, *Adv. Mater.*, 2009, **21**, 1712–1715.
- 2 H. Daemi, S. Rajabi-Zeleti, H. Sardon, M. Barikani, A. Khademhosseini and H. Baharvand, *Biomaterials*, 2016, **84**, 54–63.
- 3 E. Ducrot and C. Creton, *Adv. Funct. Mater.*, 2016, **26**, 2482–2492.
- 4 E. Ducrot, Y. Chen, M. Bulters, R. P. Sijbesma and C. Creton, *Science*, 2014, **344**, 186–189.
- 5 Y. Du, M. Yu, J. Ge, P. X. Ma, X. Chen and B. Lei, *Adv. Funct. Mater.*, 2015, **25**, 5016–5029.
- 6 D. A. Norman and R. E. Robertson, *Polym.*, 2003, **44**, 2351–2362.
- 7 B. Fiedler, F. H. Gojny, M. H. G. Wichmann, M. C. M. Nolte and K. Schulte, *Compos. Sci. Technol.*, 2006, **66**, 3115–3125.
- 8 H. P. S. Abdul Khalil, A. H. Bhat and A. F. Irena Yusra, *Carbohydr. Polym.*, 2012, **87**, 963–979.
- 9 R. J. Moon, A. Martini, J. Nairn, J. Simonsen and J. Youngblood, *Chem. Soc. Rev.*, 2011, **40**, 3941–3994.
- 10 D. Klemm, B. Heublein, H. P. Fink and A. Bohn, *Angew. Chem., Int. Ed.*, 2005, **44**, 3358–3393.
- 11 L. Vaysse, F. Bonfils, J. Sainte-Beuve and M. Cartault, in *Polymer Science: A Comprehensive Reference*, ed. K. M. Möller, Elsevier, Amsterdam, 2012, pp. 281–293, DOI: 10.1016/B978-0-444-53349-4.00267-3.
- 12 A. Ali Shah, F. Hasan, Z. Shah, N. Kanwal and S. Zeb, *Int. Biodeterior. Biodegrad.*, 2013, **83**, 145–157.
- 13 A. I. Isayev, in *Chemistry, Manufacture and Applications of Natural Rubber*, ed. S. Kohjiya and Y. Ikeda, Woodhead Publishing, 2014, pp. 395–435, DOI: 10.1533/9780857096913.3.395.
- 14 B. P. Mooney, *Biochem. J.*, 2009, **418**, 219–232.
- 15 Z. Peng, C. Feng, Y. Luo, Y. Li and L. X. Kong, *Carbon*, 2010, **48**, 4497–4503.
- 16 Y. Mao, S. Wen, Y. Chen, F. Zhang, P. Panine, T. W. Chan, L. Zhang, Y. Liang and L. Liu, *Sci. Rep.*, 2013, **3**, 2508.

- 17 R. Peter, V. R. Vijay, S. Ramakrishnan, R. Sukumar and A. R. R. Menon, *Appl. Clay Sci.*, 2015, **105–106**, 186–191.
- 18 S. A. Riyajan, *Carbohydr. Polym.*, 2015, **134**, 267–277.
- 19 C. Zhang, Y. Dan, J. Peng, L. S. Turng, R. Sabo and C. Clemons, *Adv. Polym. Technol.*, 2014, **33**, 21448.
- 20 P. M. Visakh, S. Thomas, K. Oksman and A. P. Mathew, *Composites, Part A*, 2012, **43**, 735–741.
- 21 Y. Ikeda, T. Phakkeeree, P. Junkong, H. Yokohama, P. Phinyocheep, R. Kitano and A. Kato, *RSC Adv.*, 2017, **7**, 5222–5231.
- 22 S. Xu, J. Gu, Y. Luo, D. Jia and L. Yan, *Polym. Compos.*, 2015, **36**, 861–868.
- 23 E. Trovatti, A. J. F. Carvalho, S. J. L. Ribeiro and A. Gandini, *Biomacromolecules*, 2013, **14**, 2667–2674.
- 24 P. Visakh, S. Thomas, K. Oksman and A. P. Mathew, *BioResources*, 2012, **7**, 2156–2168.
- 25 E. Abraham, B. Deepa, L. A. Pothan, M. John, S. S. Narine, S. Thomas and R. Anandjiwala, *Cellulose*, 2013, **20**, 417–427.
- 26 N. Amiralian, P. Annamalai, P. Memmott and D. Martin, *Cellulose*, 2015, **22**, 2483–2498.
- 27 N. Amiralian, P. K. Annamalai, P. Memmott, E. Taran, S. Schmidt and D. J. Martin, *RSC Adv.*, 2015, **5**, 32124–32132.
- 28 H. P. S. Abdul Khalil, Y. Davoudpour, M. N. Islam, A. Mustapha, K. Sudesh, R. Dungani and M. Jawaid, *Carbohydr. Polym.*, 2014, **99**, 649–665.
- 29 X. Wu, T. F. Lin, Z. H. Tang, B. C. Guo and G. S. Huang, *EXPRESS Polym. Lett.*, 2015, **9**, 672–685.
- 30 D. Ballner, S. Herzele, J. Keckes, M. Edler, T. Griesser, B. Saake, F. Liebner, A. Potthast, C. Paulik and W. Gindl-Altmutter, *ACS Appl. Mater. Interfaces*, 2016, **8**, 13520–13525.
- 31 N. Yousefi Shivyari, M. Tajvidi, D. W. Bousfield and D. J. Gardner, *ACS Appl. Mater. Interfaces*, 2016, **8**, 25520–25528.
- 32 A. A. Rowe, M. Tajvidi and D. J. Gardner, *J. Therm. Anal. Calorim.*, 2016, **126**, 1371–1386.
- 33 J. A. Sirvio, M. Visanko and H. Liimatainen, *Green Chem.*, 2015, **17**, 3401–3406.
- 34 K. Ahmed, S. S. Nizami, N. Z. Raza and K. Shirin, *Adv. Mater. Phys. Chem.*, 2012, **2**, 90–97.
- 35 S. Y. Oh, D. I. Yoo, Y. Shin, H. C. Kim, H. Y. Kim, Y. S. Chung, W. H. Park and J. H. Youk, *Carbohydr. Res.*, 2005, **340**, 2376–2391.
- 36 C. F. Liu, R. C. Sun, A. P. Zhang, J. L. Ren and Z. C. Geng, *Polym. Degrad. Stab.*, 2006, **91**, 3040–3047.
- 37 M. Fan, D. Dai and B. Huang, in *Fourier Transform - Materials Analysis*, ed. S. M. Salih, InTech, 2012, vol. 1, ch. 3, pp. 45–68.
- 38 D. Roy, J. T. Guthrie and S. Perrier, *Soft Matter*, 2008, **4**, 145–155.
- 39 C. Thulasimani, S. Ramesh, K. Ramesh and H. Salmah, *Asia-Pac. J. Chem. Eng.*, 2015, **10**, 716–723.
- 40 C. M. Oioescue, M. C. Popescu, G. Singurel, C. Vasile, D. S. Argyropoulos and S. Willfor, *Appl. Spectrosc.*, 2007, **61**, 1168–1177.
- 41 W. Lan, C.-F. Liu, F.-X. Yue and R.-C. Sun, in *Cellulose - Fundamental Aspects*, ed. T. V. D. Ven and L. Godbout, 2013, DOI: 10.5772/52517.
- 42 R. Marchessault, *Pure Appl. Chem.*, 1962, **5**, 107–130.
- 43 M. Schwanninger, J. Rodrigues, H. Pereira and B. Hinterstoisser, *Vib. Spectrosc.*, 2004, **36**, 23–40.
- 44 Y. Zidan, N. El Hadidi and M. Mohamed, *Mediterranean, Archaeology, Archaeometry*, 2016, **16**, 1–11.
- 45 C. Y. Tang, Y.-N. Kwon and J. O. Leckie, *Desalination*, 2009, **242**, 149–167.
- 46 A. A. Shamsuri and R. Daik, *BioResources*, 2012, **7**, 4760–4775.
- 47 S. Zhang, Z. Ren, S. He, Y. Zhu and C. Zhu, *Spectrochim. Acta, Part A*, 2007, **66**, 188–193.
- 48 J. F. Ma, K. Tamai, N. Yamaji, N. Mitani, S. Konishi, M. Katsuhara, M. Ishiguro, Y. Murata and M. Yano, *Nature*, 2006, **440**, 688–691.
- 49 W. H. Casey, S. D. Kinrade, C. T. G. Knight, D. W. Rains and E. Epstein, *Plant, Cell Environ.*, 2004, **27**, 51–54.
- 50 N. Amiralian, P. K. Annamalai, C. Fitzgerald, P. Memmott and D. J. Martin, *Ind. Crops Prod.*, 2014, **59**, 241–247.
- 51 J. Gustafsson, L. Ciofica and J. Peltonen, *Polym.*, 2003, **44**, 661–670.
- 52 J. Bañuls-Ciscar, D. Pratelli, M.-L. Abel and J. F. Watts, *Surf. Interface Anal.*, 2016, **48**, 589–592.
- 53 Y. Ma, S. Asaadi, L.-S. Johansson, P. Ahvenainen, M. Reza, M. Alekhina, L. Rautkari, A. Michud, L. Hauru, M. Hummel and H. Sixta, *ChemSusChem*, 2015, **8**, 4030–4039.
- 54 M. George, P. G. Mussone and D. C. Bressler, *Ind. Crops Prod.*, 2014, **53**, 365–373.
- 55 R. W. Truss, B. Wood and R. Rasch, *J. Appl. Polym. Sci.*, 2016, **133**, 43023.
- 56 S. Alila, A. M. Ferraria, A. M. Botelho do Rego and S. Boufi, *Carbohydr. Polym.*, 2009, **77**, 553–562.
- 57 G. Beamson and D. Briggs, *High Resolution XPS of Organic Polymers: The Scienta ESCA300 Database*, Wiley, 1992.
- 58 S. Yang, L. Liu, Z. Jia, W. Fu, D. Jia and Y. Luo, *EXPRESS Polym. Lett.*, 2014, **8**, 425–435.
- 59 C. C. Ho and M. C. Khew, *Langmuir*, 2000, **16**, 1407–1414.
- 60 C. W. Extrand and A. N. Gent, *Rubber Chem. Technol.*, 1988, **61**, 688–697.
- 61 M. A. Hubbe, O. J. Rojas, L. A. Lucia and M. Sain, *BioResources*, 2008, **3**, 929–980.
- 62 Z. Bao, C. Flanigan, L. Beyer and J. Tao, *J. Appl. Polym. Sci.*, 2015, **132**, 41521.
- 63 W. P. Flauzino Neto, M. Mariano, I. S. V. da Silva, H. A. Silvério, J.-L. Putaux, H. Otaguro, D. Pasquini and A. Dufresne, *Carbohydr. Polym.*, 2016, **153**, 143–152.
- 64 D. Riyapan, S.-A. Riyajan and A. Kowalczyk, *Polym. Bull.*, 2015, **72**, 671–691.
- 65 S. A. Riyajan, D. Riyapan and P. Tangboriboonrat, *J. Biobased Mater. Bioenergy*, 2014, **8**, 403–408.
- 66 S. Wang, X. Peng, L. Zhong, S. Jing, X. Cao, F. Lu and R. Sun, *Carbohydr. Polym.*, 2015, **117**, 133–139.
- 67 P. K. Annamalai, K. L. Dagnon, S. Monemian, E. J. Foster, S. J. Rowan and C. Weder, *ACS Appl. Mater. Interfaces*, 2014, **6**, 967–976.
- 68 A. Bendahou, H. Kaddami and A. Dufresne, *Eur. Polym. J.*, 2010, **46**, 609–620.